Appendix A: Emission maps in different rotational transitions of C_4H, C_3N, HC_3N, and HC_5N

The radicals C_4H and C_3N have several rotational transitions $N - (N - 1)$ in the λ 3 mm band, each split into two closely spaced spin-rotation doublets of nearly equal intensity labeled as "a" and "b" (see Figs. A.1 and A.2), while the cyanopolyynes HC_3N and HC_5N also have several rotational transitions within the frequency range covered (see Fig. A.5). Here we present the emission maps of each individual line and discuss whether the different lines of a given species have brightness distributions significantly different among them and whether the individual maps show any anomalies.

In Figs. A.1 and A.2 we show the brightness distributions of each component of the doublet rotational transitions for the radicals C_4H ($N = 9 - 8$ through $N = 12 - 11$) and C_3N (from $N = 9 - 8$ to $N = 11 - 10$). The upper level energies of these transitions, in the range 20.5-35.6 K for C_4H and 21.4-31.3 K for C_3N, do not differ enough so to expect important differences in the excitation, which could in turn lead to significantly distinct emission distributions. Apart from some slight differences in the absolute intensities, the brightness distributions of the lines of C_3N are very similar both in the locations of the maxima and the arrangement of the arcs that shape the overall ring. The same is also true for C_4H, with the exception of the anomaly in the map of the $N = 12 - 11$ b transition. This line shows the same ring structure seen in the rest of the C_4H lines, but there is also a compact component centered on the star that is not resolved by the $1''.14 \times 0''.98$ synthesized beam. If the compact emission were to arise from C_4H, it would be very difficult to explain why it is only seen in this line while there is no hint of it in the maps of the other seven lines of C_4H. Instead this compact emission arises from CO $J = 1 - 0$ in its first vibrationally excited state, whose rest frequency, 115221.754 MHz, is only 0.7 MHz away from that of the $N = 12 - 11$ b transition of C_4H. Emission from CO in the vibrational state $v = 1$ had been detected in IRC +10216 in the pure rotational transitions $J = 2 - 1$ and $J = 3 - 2$ with the Submillimeter Array (SMA) by Patel et al. (2009). The emission in these lines remains unresolved with an angular resolution of $\sim 2''$, while that from the $J = 1 - 0$ line we have detected remains

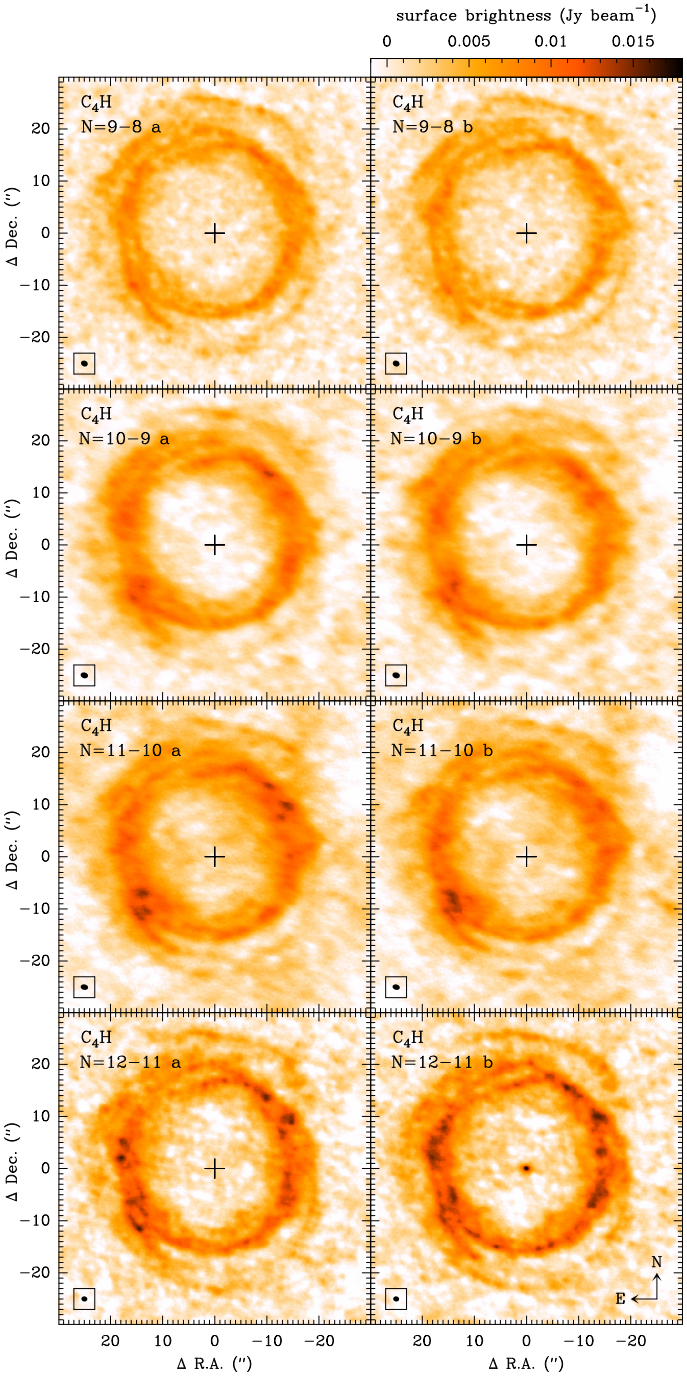

Fig. A.1. Brightness distributions of the $N = 9 - 8$ through $N = 12 - 11$ spin-rotation doublets of C_4H, averaged over the central 3 km s^{-1} of each line. The size ($\sim 1''$ for all lines) and shape of the synthesized beam is shown in the bottom left corner of each panel. Maps are centered on the position of the star, indicated by a cross. The compact unresolved emission centered on the star in the panel corresponding to the C_4H $N = 12 - 11$ b line arises from the $v = 1$ $J = 1 - 0$ transition of CO.

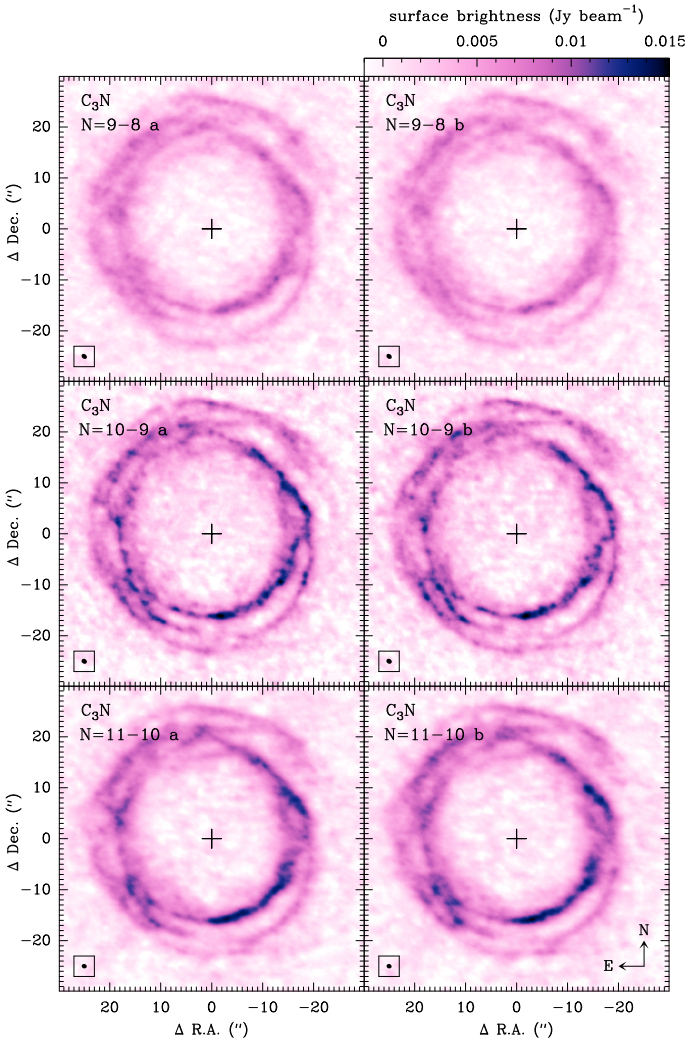

Fig. A.2. Brightness distributions of the $N = 9 - 8$ through $N = 11 - 10$ spin-rotation doublets of C_3N, averaged over the central 3 km s^{-1} of each line. The size ($\sim 1''$ for all lines) and shape of the synthesized beam is shown in the bottom left corner of each panel. Maps are centered on the position of the star, indicated by a cross.

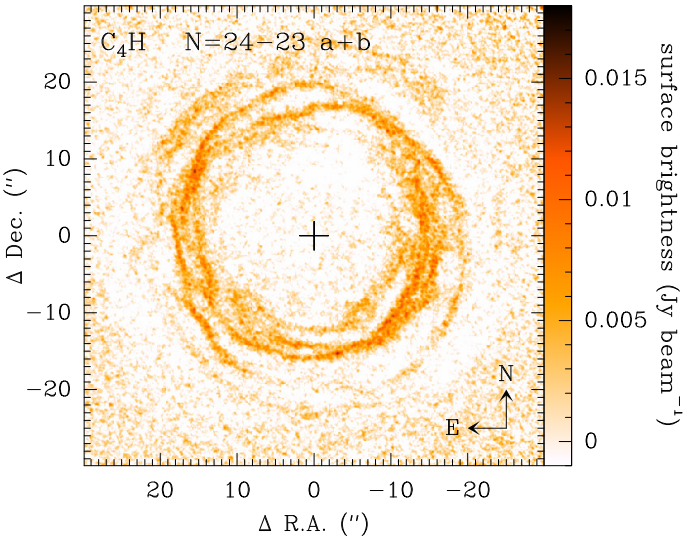

Fig. A.3. ALMA Cycle 2 brightness distribution of the $N = 24-23$ transition of C_4H at $V_{LSR} = V_{sys}$, where the two spin-rotation components have been stacked. The synthesized beam is $0\farcs37 \times 0\farcs34$ and the rms per 0.62 km s^{-1} channel is 4.8 mJy beam^{-1}. The map is centered on the position of the star, indicated by a cross.

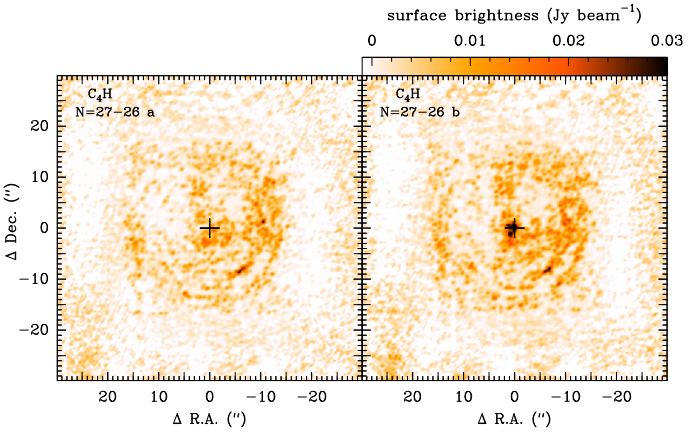

Fig. A.4. ALMA Cycle 0 brightness distributions of the two spin-rotation components of the $N = 27-26$ transition of C_4H, averaged over the central 4 km s^{-1} of each line. The synthesized beam is $0\farcs77 \times 0\farcs61$ and the rms per 4 km s^{-1} channel is 1.3 mJy beam^{-1}. Maps are centered on the position of the star, indicated by a cross. Note that most of the ring structure is lost because this emission lies well outside the primary beam of ∼23″, and that a compact structure centered on the star is only clearly visible in the N = 27-26 b line.

unresolved with an angular resolution of ∼1″, indicating that the emission from CO $v = 1$ arises from a region closer than $\sim 10^{15}$ cm ($\sim 25\ R_*$) to the star. It is also worth noting that recently, emission from the pure rotational transition $J = 3-2$ of CO in the vibrational state $v = 1$ has been observed using ALMA with subarcsecond resolution in five additional AGB stars (Khouri et al. 2016), pointing to a line-formation region smaller than $\sim 10\ R_*$ in radius.

In Fig. A.3 we show the brightness distribution of C_4H in the rotational transition $N = 24-23$, lying at 228.3 GHz. The map corresponds to an average of the two spin-rotation components in the central velocity channel and was obtained with ALMA band 6 during Cycle 2. More details on these observations will be given elsewhere (Guélin et al., in preparation). The map of this line shows the same structure of thin shells and inter-crossing arcs displayed by the λ 3 mm lines of C_4H, but seen at a higher angular resolution, ∼0.3″, and with a higher contrast because part of the extended emission filtered out by the interferometer has not been recovered owing to the lack of short-spacings data.

According to the ALMA maps of the four doublet lines of C_4H shown in Fig. A.1 and the transition shown in Fig. A.3, the emission of C_4H is clearly restricted to the outer hollow shell, with no emission arising from the surroundings of the star. Cooksy et al. (2015), however, find in their SMA maps of the doublet line $N = 27-26$ of C_4H that there is compact emission centered on the star. This doublet, lying at 256.9 GHz, has been covered in our ALMA Cycle 0 observations of IRC +10216, a large portion of which has been already published (Cernicharo et al. 2013; Velilla Prieto et al. 2015; Agúndez et al. 2015; Quintana-Lacaci et al. 2016). As shown in Fig. A.4, at velocities around $V_{LSR} = V_{sys}$ the outer ring is barely seen in our ALMA Cycle 0 data because the size of the ring is larger than the field of view (∼23″) and thus this emission is not properly sampled. In contrast, compact emission around the star is clearly seen, but only in the b component of the $N = 27-26$ doublet and not in the a component. This was not recognized in the data shown by Cooksy et al. (2015) because these authors stacked the maps of the two components of the doublet to improve the sensitivity. As shown for the C_4H $N = 12-11$ doublet in Fig. A.1, it is more likely that the compact emission seen in the map of the $N = 27-26$ b component does not arise from C_4H but rather from a different carrier that has a transition which accidentally coincides with the $N = 27-26$ b component of C_4H. At this stage we do not have a fully convincing assignment for this line, but the emission maps of the entire set of λ 3 and 1 mm lines of C_4H strongly support that this species is only present in the outer shell and not in regions close to the star.

There are several rotational transitions of cyanoacetylene and cyanodiacetylene in the λ 3 mm band observed here. For HC_3N just three lines are covered, from $J = 10-9$ to $J = 12-11$. These transitions have similar upper level energies, in the range 24.0-34.1 K, and thus, like the carbon chain radicals, we do not expect great differences in their excitation, and thus in their emission distribution. The maps of brightness of these three lines, centered on the systemic velocity, are shown in the top panels of Fig. A.5, where it can be seen that there are indeed no substantive differences.

For HC_5N, 12 rotational lines, ranging from $J = 32-31$ through $J = 43-42$, have been covered. These transitions involve upper levels with energies from 67.5 to 120.9 K, i.e., substantially higher than those involved in the HC_3N transitions. The emission maps of each individual line of HC_5N (see a sample in the lower panels of Fig. A.5) show that there is a noticeable decline in intensity with increasing J. This decrease in line intensity can be understood as a consequence of a less efficient excitation of levels of increasing energy in the outer shell at ∼15″ from the star, where the gas kinetic temperature and the volume density of particles are expected to be just 10-30 K and $(1-5) \times 10^4$ cm^{-3}. As such, one might reasonably expect some radial shift in the emission peak between low-J and high-J lines, the latter being more easily excited at shorter radii because of the higher temperatures and densities. At current angular resolution and sensitivity of the measurements, there is no evidence of such shift among the λ 3 mm lines of HC_5N, whose emission distributions appear quite similar. It therefore seems that the structure of density enhancements in the form of arcs and shells is much more important than differential excitation effects in shaping the brightness distributions. The same is found for C_4H, C_3N, and HC_3N, where the transitions that we mapped involve levels with more similar energies. Therefore we conclude that regardless of the particular λ 3 mm transition adopted for any of the carbon chains studied here, the brightness distribution is a good proxy of the spatial distribution of the species. Keller et al. (2015) have recently presented preliminary results on ∼1″ angular resolution VLA maps of cm-wavelength rotational lines of carbon chains in IRC +10216. These transitions involve rotational levels with energies significantly below those associated to the λ 3 mm lines presented here, and thus it will be interesting to see if there are significant differences in the distribution of the emission of cm- and 3 mm-wavelength lines that could arise from excitation effects.

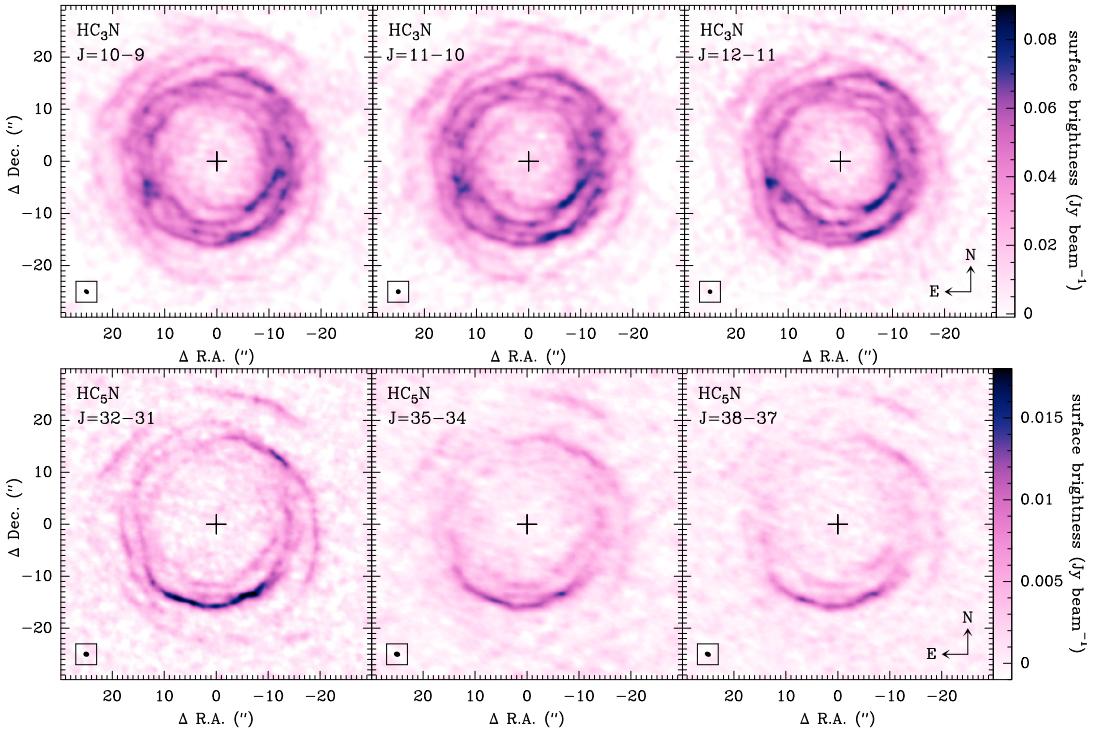

Fig. A.5. Brightness distributions of the $J = 10 - 9$, $J = 11 - 10$, and $J = 12 - 11$ lines of HC_3N (top panels), and $J = 32 - 31$, $J = 35 - 34$, and $J = 38 - 37$ lines of HC_5N (bottom panels), averaged over the central 3 km s^{-1} of each line. The size ($\sim 1''$ for all lines) and shape of the synthesized beam is shown in the bottom left corner of each panel. The maps are centered on the position of the star, indicated by a cross.